CHAPTER IV
RESULTS AND DISCUSSION

To examine the hydrogen diffusion through industrially relevant metal such as carbon steel and Hastelloy, the diffusion of hydrogen was measured using gas phase permeation techniques. A schematic of the apparatus is shown in Chapter 3. The hydrogen permeation rate through the tube wall was determined by the rate of hydrogen pressure decrease with time measured by pressure transducer. All tube assemblies were subjected to leak tests for two days at room temperature before proceeding with permeation tests. The hydrogen pressure reduction was measured with time to determine the rate of mass transport of hydrogen through the tube. The decrease of pressure assumes all hydrogen lost passes through the metal and no hydrogen is trapped within the metal.

This study was also focused on the effect of a palladium film applied to the outside steel surface on the hydrogen diffusion through the tube. Palladium has advantages as a coating because of its catalytic surface. The palladium increases the rate of hydrogen diffusion from intrinsic steels. The similar tube was coated by electroless plating techniques. The results of the tube with and without the presence of palladium on the surface were compared the diffusion rate. Table 4.1 presents the summary of all tests that were carried on for the research.

Table 4.1 Summary of tests performed

Test No.	Scope	Material	Surface condition	Temperature (°C)	Duration (hr)
1	Minimum Temperature Limit	CS	Outer Oxide layer	MTL	359
2	Temperature Effect	CS	Outer Oxide layer	150	190
3	Temperature Effect	CS	Outer Oxide layer	250	46
4	Catalyst coating Effect	CS	Catalyst coating on the outside surface	150	63
5	Catalyst coating Effect	CS	Catalyst coating on the outside surface	250	23
6	Minimum Temperature Limit	Hastelloy	Outer Oxide layer	MTL	48
7	Temperature Effect	Hastelloy	Outer Oxide layer	250	185
8	Temperature Effect	Hastelloy	Outer Oxide layer	335	74
9	Catalyst coating Effect	Hastelloy	Catalyst coating on the outside surface	250	185
10	Catalyst coating Effect	Hastelloy	Catalyst coating on the outside surface	335	74

RESULTS

4.1 Hydrogen Permeation through Carbon Steel

4.1.1 Minimum Temperature Limit

The Minimum Temperature Limit (MTL) is the temperature above which hydrogen will permeate through the steel. Tests were conducted at various temperatures to find the MTL.
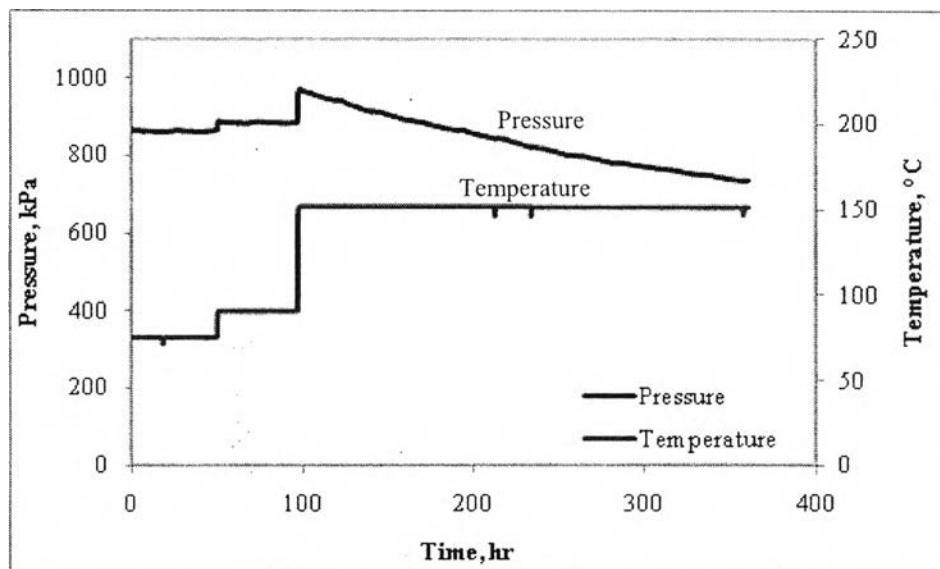
Figure 4.1 Pressure observed as a function of time to determine the lowest temperature of hydrogen permeation of a carbon steel tube.

Hydrogen was introduced into the system 864.74 kPa at room temperature. In order to study the threshold temperature for hydrogen diffusion, the testing apparatus was heated. The testing temperature was increased by 15°C increments until the minimum temperature limit is achieved. The first test was performed at 75°C and the second test at 90°C. These first two temperatures gave no measurable permeation of hydrogen through the tube specimen. The results are shown in Table 4.2 "No change" written in the table means that there was no measurable change, in the pressure over the time allowed. The set point temperature was adjusted

to 150°C. The hydrogen pressure decreased from 964.3 kPa to 732.2 kPa in 264.4 hr. The decreasing rate is 0.646 kPa/hr.

Table 4.2 Summary of MTL tests performed

Test Temp. (°C)	Initaial P (kPa)	Final P (kPa)	D_{app} Based on Fick's law $(m^2 s^{-1})$	D_{app} Based on Sievert's law $(m^2 s^{-1})$	Resistance $(s\ m^{-1})$	Decrease rate (kPa/hr)
75	865.10	864.88	-	-	-	No change
90	889.09	886.83	-	-	-	No change
150	964.36	732.28	2.48×10^{-13}	2.00×10^{-11}	3.02×10^9	0.646

Therefore, the MTL is between $90 \leq T \leq 150$°C. The apparent diffusivity of the minimum temperature of 150°C is 2.48×10^{-13} $m^2\ s^{-1}$ and the resistance is 3.02×10^9 s m^{-1}. The results are summarized in Table 4.2. Hydrogen mobility should increase with temperature. This is probably due to the increase in hydrogen dissociation into the atomic state. The diffusion of atomic hydrogen increases with temperature. The kinetics also increases as the temperature increase. Equilibrium is more favorable when the temperature increases.

4.1.2 Hydrogen Diffusion through passive oxide layer

The carbon steel outside surface for this experiment was as received from the manufacturer. This condition of the surface would be in normal use. The outside passive oxide film was therefore allowed to form spontaneously. The inside surface of the tubular specimen was exposed to hydrogen purging to remove the oxide layer. The purging step was conducted by passing 7.7 ml/min of hydrogen gas through the tube for 5 days at the temperature of 325°C. This purging step was carried out for all tests. The treatment has potential to increase oxide layer on the outside surface.

For the tests hydrogen was charged into the tube at an initial pressure of 790 kPa and 25°C. A leak check was performed for the first two days. After no

leak was observed, the tube was heated to the desired temperature. The temperature was kept constant throughout the experiment.

The effect of temperature was determined by two temperatures of 150°C and 250°C. From previous diffusion data, the hydrogen diffusion rate has been found to increase temperature (Paneni, 1969; Cao, 2002; Mamani, 2005). Figure 4.2 presents the decrease in hydrogen pressure with time for 150 and 250°C with an oxide layer on the outside and the oxide layer removed from the inside.
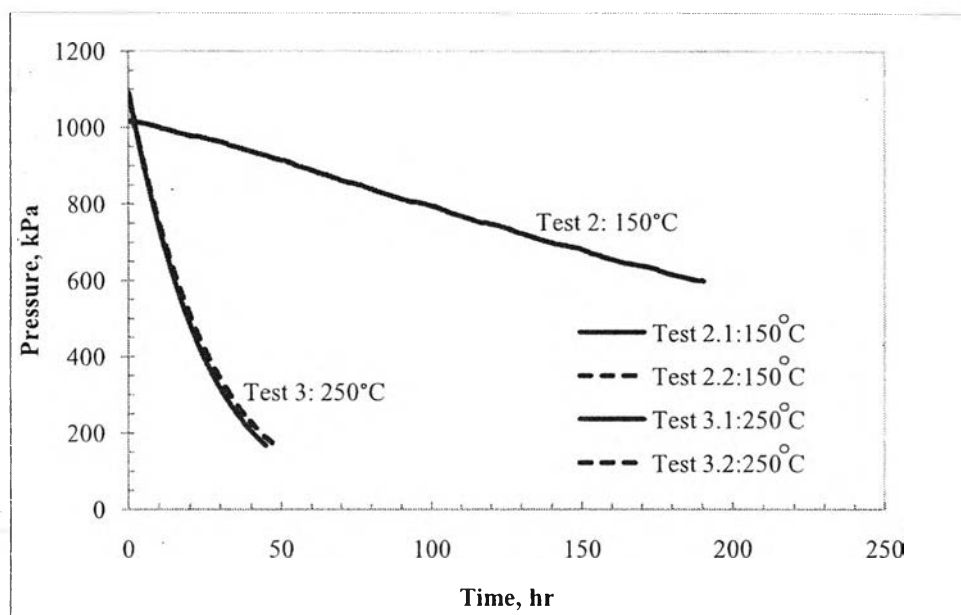
Figure 4.2 The change in hydrogen pressure inside the tube membrane with time at the testing temperature of 150°C and 250°C with the oxide layer on the outside and oxide layer removed from the inside.

It can be seen from Figure 4.2 that hydrogen diffusion rate increases as temperature increases, for the same sample surface conditions, test no. 2 and 3 were used to compare. The repeated tests are in good agreement with the prior test. At two temperatures display the high repeatability. The results are summarized in Table 4.3. The higher temperature (250°C) gave a higher rate of diffusion of hydrogen.

Table 4.3 Summary of experimental data and constant value calculation

Test no.	Temp. (°C)	Initaial P (kPa)	Final P (kPa)	D_{app} Based on Fick's law ($m^2 s^{-1}$)	D_{app} Based on Sievert's law ($m^2 s^{-1}$)	Resistance ($s\, m^{-1}$)
2.1	150	1017.2	598.3	6.65×10^{-13}	1.31×10^{-6}	1.13×10^{9}
2.2	150	1003.6	792.7	3.37×10^{-13}	7.12×10^{-7}	2.23×10^{9}
3.1	250	1089.7	165.8	9.32×10^{-12}	3.99×10^{-6}	8.07×10^{7}
3.2	250	1087.3	113.3	7.50×10^{-12}	2.96×10^{-6}	1.00×10^{8}

Table 4.3 presents the apparent diffusivity and the hydrogen transport resistance through the carbon steel. The apparent diffusivity and the overall resistance were computed from the rate of pressure decrease. The calculations are shown in Appendix E and F. The diffusivity is temperature dependent and increased with temperature. The tests at both temperatures are repeated. Consider the diffusivity and resistance, the value displays small variation. The repeated tests have lower diffusivity and higher resistance. It may be caused from the outside oxide thickness changes overtime.
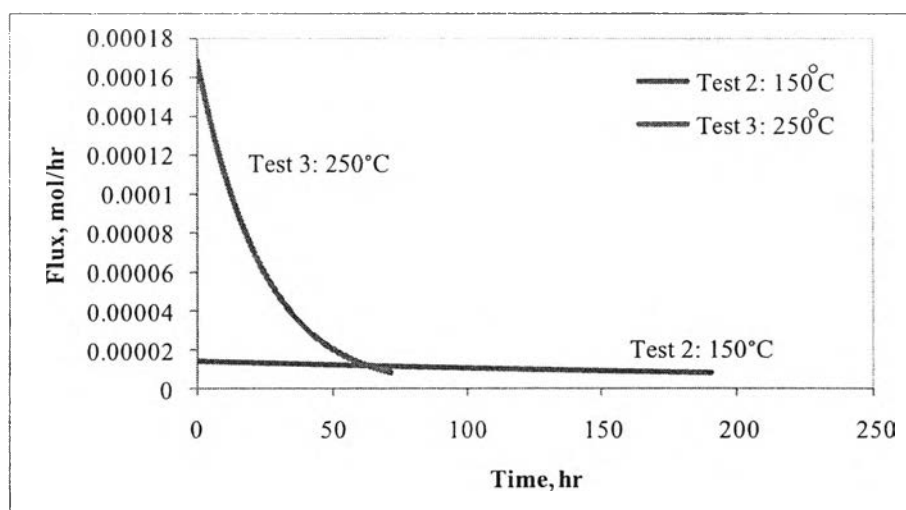

Figure 4.3 Permeation flux as a function of time for the two temperatures.

Figure 4.3 shows the relationship between the permeation fluxes with time. Flux is defined as the rate of hydrogen passing through the tube. The least square analysis was used for the calculation of flux as a function of time. The

calculation is presented in Appendix C. The data shows that 150°C yields essentially a constant rate of diffusion. The diffusion rate at 150°C gradually decreases with the constant rate throughout the experiment. For the case of higher temperature as 250°C, the rate of hydrogen diffusion at 250°C drops rapidly at the beginning as the curve shows and the rate is slower when the driving pressure is small. The higher temperature gives the higher flux of permeation.

(a)   (b)
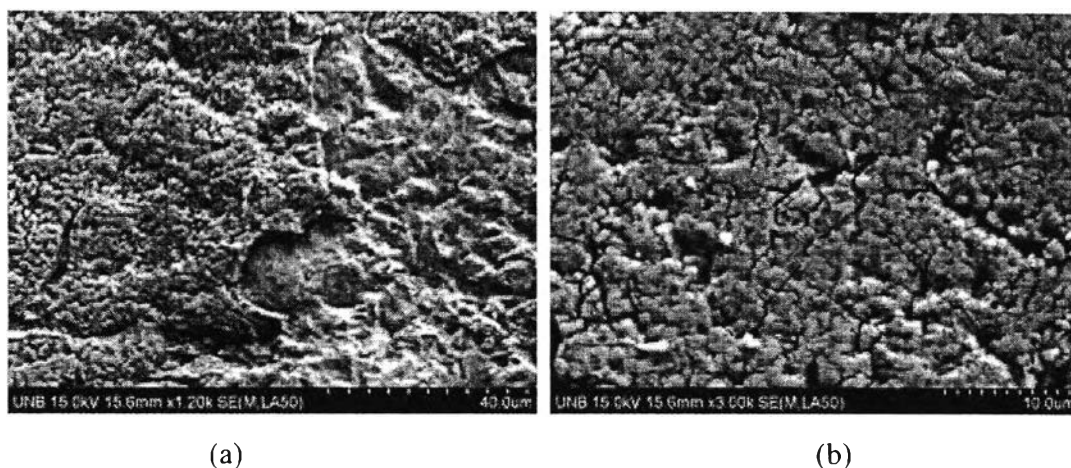
Figure 4.4 FESEM images of the oxide film deposited on the carbon steel outside surface during experiment performed (Magnification, 1300X for (a) and 4000X for (b)).

The deposit of oxide film on the outside surface of the carbon steel tube was created by exposed to air during the experiments conducted as shown in Figure 4.4. The morphology can be seen from FESEM analyses. The film presents crack patterns. It is believed that hydrogen diffuses through those cracks.

4.1.3   Hydrogen Diffusion through Palladium coated layer

Hydrogen diffusion through metal was affected by the presence of surface films on both input and output side of the specimen. The passage rate of hydrogen through the metal was delayed when the oxide layer presented. Exposure of metals and alloys to air at high temperature leads to the formation of oxide films. Air-formed oxide films on metals impede either hydrogen entry into the metal or hydrogen exit from the metal. The oxide film retards the adsorption process, whereby hydrogen molecules in the gas phase dissociate on the solid surface, and the

desorption process, whereby adsorbed hydrogen atoms recombine and released as molecules. These two processes are known as surface effects and under certain conditions they may control the permeation rate (surface-limited permeation).

It is well known to use of palladium films to allow hydrogen entry and protects the cleaned surface from oxidation. It has been used because palladium presents high hydrogen selectivity. Orani et al.(2000) noticed in their research that palladium lattice has the lower energy sites so that these are preferentially occupied by hydrogen.

To investigate the role of palladium catalyst on hydrogen permeation rate, palladium film were coated on the carbon steel surface by electroless plating technique. Then the plated specimen was performed the hydrogen permeation experiments as the same procedure as the oxidized surfaces in section 4.1.2. The results were used to compare the hydrogen permeation rate with the catalyst coated surface.
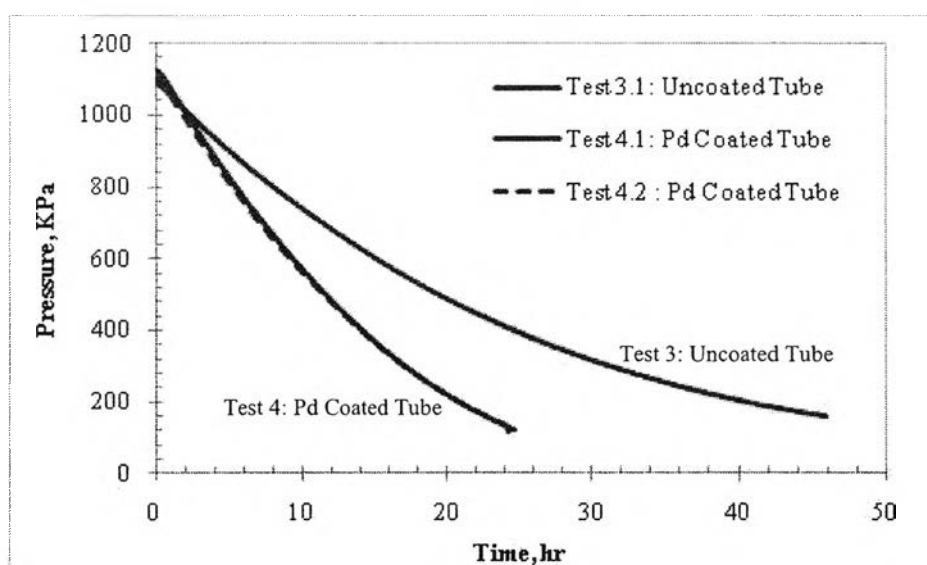
Figure 4.5 The comparison in hydrogen pressure with time at the test temperature of 150°C with and without palladium coated on the outside.

The hydrogen pressure reduction with time of the tube coated with palladium was illustrated in Figure 4.5. It can be seen that the pressure reduction rate of the coated tube was faster than the uncoated tube. For the case of the palladium

coated tube spent 62.4 hours, whereas the uncoated specimen spent 190.5 hours. The outside surface after coating reduces the permeation time about 128.2 hours to reach the same final pressure. Test 4.1 and 4.2 demonstrate the high repeatability as shown in the similar curve.
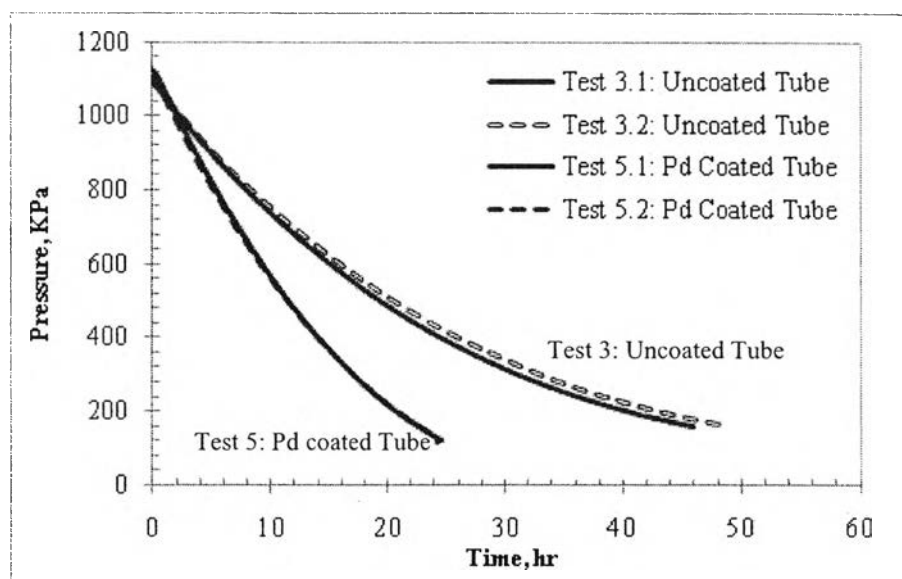
Figure 4.6 The comparison in hydrogen pressure with time at the test temperature of 250°C with and without palladium coated on the outside.

The results obtained for 250°C tests, which are plotted the hydrogen partial pressure as a function of time, are reported in Figure 4.6. The experimental data demonstrate that hydrogen permeation rate through the coated specimen was increased compared to the uncoated specimen. The hydrogen partial pressure of the coated tube was drastically decreased with time. The rate was affected by the palladium coated on the outside. For example, in the case of test 3.1 compare to 5.1 the palladium coated tube spent 22.6 hours, whereas the uncoated specimen spent 45.9 hours. The palladium catalyst coating on the outside surface can increase the rate by the factor of two. As considered the behavior of diffusion curves, they demonstrate a high reproducibility. The results of the repeated test obtain the similar results. The diffusivity and resistance of these tests are displayed in table below.

**Table 4.4** Summary of experimental data and constant value calculation

Test no.	Temp. ($^\circ$C)	Initaial P (kPa)	Final P (kPa)	D_{app} Based on Fick's law ($m^2 s^{-1}$)	D_{app} Based on Sievert's law ($m^2 s^{-1}$)	Resistance (s m^{-1})
4	150	1016.42	526.69	2.05×10^{-12}	3.94×10^{-6}	3.65×10^{8}
5.1	250	1121.79	121.67	2.15×10^{-11}	8.71×10^{-6}	3.49×10^{7}
5.2	250	1104.4	161.54	2.02×10^{-11}	8.66×10^{-6}	3.71×10^{7}

4.1.4   Surface Characterizations

4.1.4.1   Palladium Coated on a carbon steel coupon

Palladium films deposited on the carbon steel tube surface were evaluated by visual inspection and surface characterization techniques. A Field Emission Scanning Electron Microscopy (FESEM) was used to examine the morphology of the palladium films. Energy Dispersive X-ray analysis (EDX) was used to verify the palladium deposition film.

The preliminary characterization was done by visual inspection and photography to determine the uniformity and the color of palladium films deposited on the surface of carbon steel ASTM A179

(a)

(b)

(c)

(d)
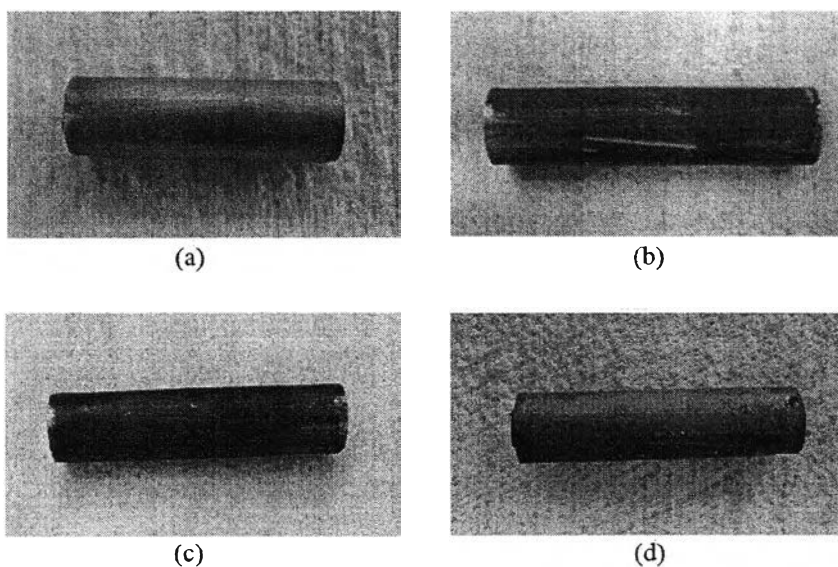
Figure 4.7: Visual picture of samples (a) Bare carbon steel, (b) After acid cleaning, (c) After activation, and (d) Palladium coated surface.

Figure 4.7 displays photographs of samples at various stages in plating. There was a significant difference of the tube surface before each step of coating. The morphology of the original metal was smoother than the surface of the sample after the film was formed. After an acid cleaning step as shown in Figure 4.7 (b) the surface was darker. The next step is a seeding step (Figure 4.7 (c)). This surface preconditioning and activation are regarded for a noncatalytic surface such as carbon steel. These steps are required for activation by generating catalytic nuclei on the tube surfaces. The activated sample had black fine powder on the surface. Figure 4.7 (d) displays the palladium film formed on the outside surfaces of the carbon steel tube. The color of the coating sample was metallic bright gray similar to the color of the bare carbon steel surface but quite rough.

(a)   (b)
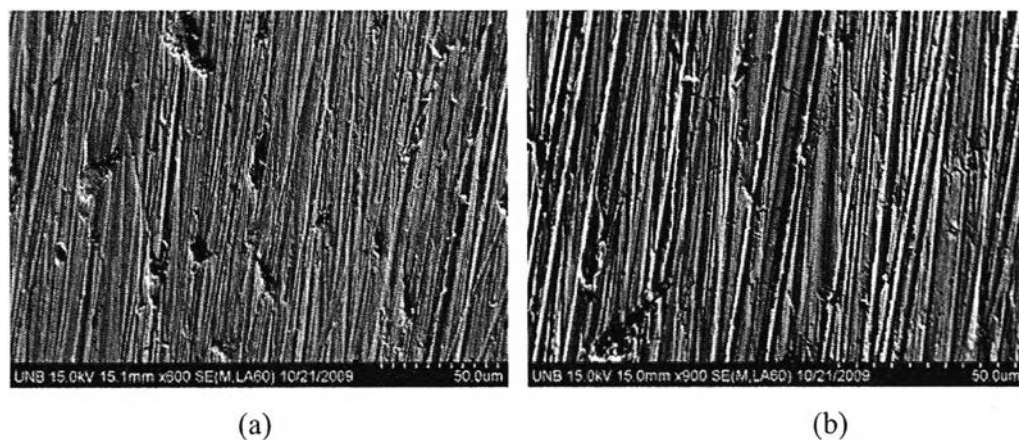
Figure 4.8 FESEM pictures of an unplated carbon steel ASTM A179 (Magnification, 600X for (a) and 900X for (b)).

The morphology of the bare carbon steel was quite rough on a microscopic scale. An unplated surface is shown in Figure 4.8 and indicates cavities. The rough surface might be caused by the mechanical polishing step. This step used sand paper 600 grit to polish.

Figure 4.9 demonstrates the surface morphology of the substrates of the activation step with Sn^{2+} and Pd^{2+} solution. The treatment with Sn^{2+} and Pd^{2+} solution produced in a large number of seeds. An energy dispersive X-ray analysis (EDX) showed those particles to be essentially palladium seeds with a small

amount of tin. Thus, the palladium nucleation on the stainless steel is believed to proceed according to the following interaction (Shu, Grandjean et al.,1993):

$$Sn^{2+} + Pd^{2+} \rightarrow Sn^{4+} + Pd^0 \qquad (50)$$

J. Shu et al. (1993) noted the adsorbed Sn^{2+} exists in a precipitated hydrolytic form on the substrate surface after the rinsing operation, and can be further replaced by Pd^0 via the redox process.


(a)   (b)
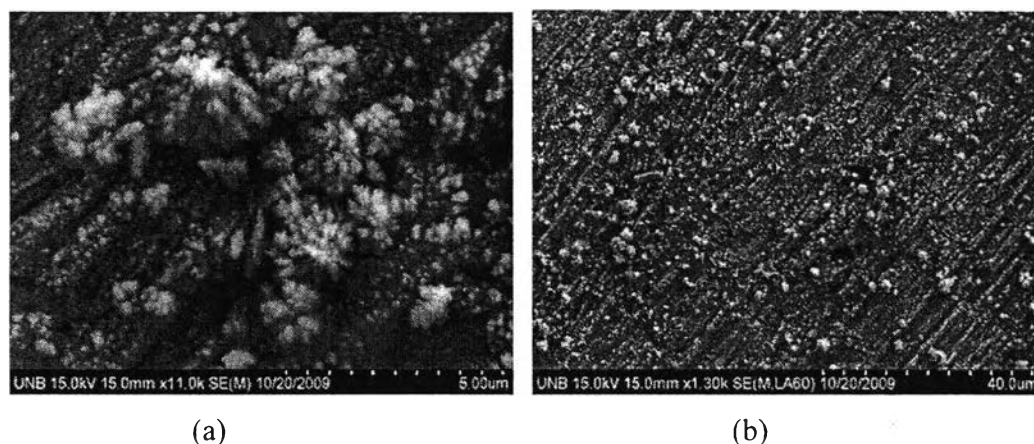
Figure 4.9 FESEM images of the activated substrate ((a) Magnification 15000X and (b) Magnification 1300X).

The deposition growth was classified into four stages: induction period, acceleration period, deceleration period and stationary period (Dogan and Kilicarslan, 2008). In the induction period, the activated substrate required a shorter time to initiate the reduction of the palladium species. The increase in the active Pd surface further promoted the catalytic deposition during the acceleration period. The deposition rate became slower in the deceleration period and finally the growth tended to saturate during the stationary period. The decrease in deposition rate is associated with the consumption of the reactants in solution
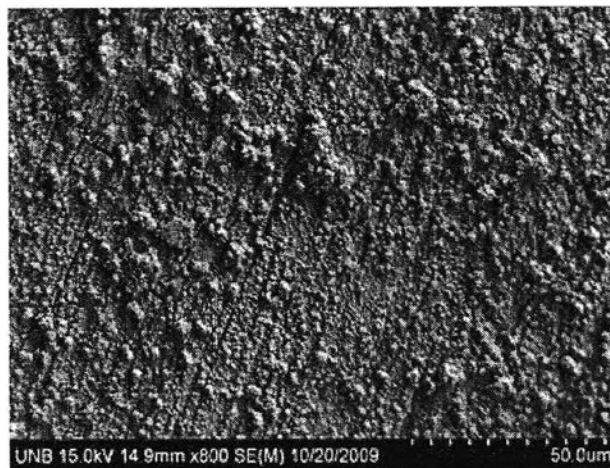
Figure 4.10 FESEM micrograph of electroless plated sample with 800X Magnification.
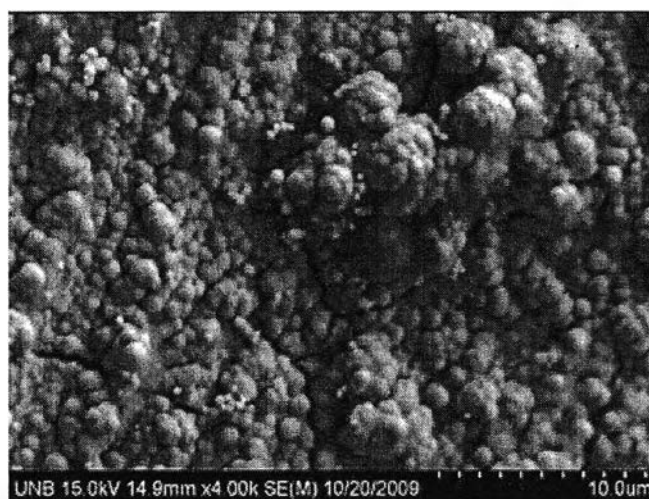

Figure 4.11 FESEM micrograph of electroless plated sample with 4000X Magnification.

UNB 15.0kV 14.9mm x15.0k SE(M) 10/20/2009   3.00um
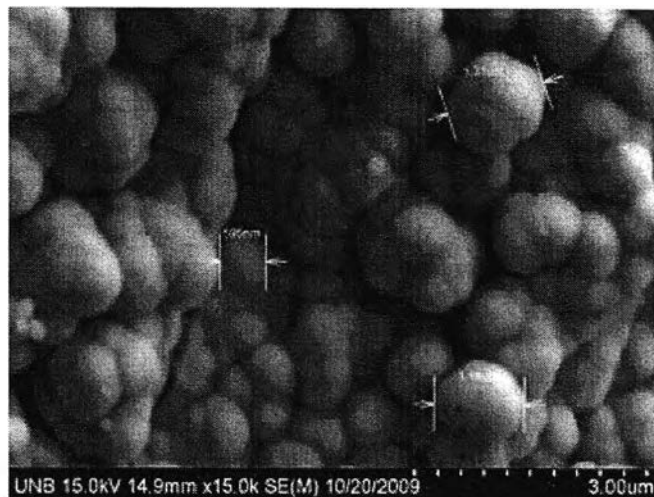
Figure 4.12 FESEM micrograph of electroless plated sample with 15000X Magnification.

      The coatings using electroless deposition were adherent and showed no macroscopic defects as shown in Figure 4.10. The sample was plated for 120 min, and revealed a uniform and coherent surface of palladium.

      The deposit exhibited a few crack patterns as shown in Figure 4.11 with higher resolution, 4000X magnifications. The crack in the palladium deposit is probably from the unsmooth surface on the substrate. The cracks also arise indirectly from mechanical stresses created in the palladium by the rough surface of the substrate(Ocken, Pound et al.,1989). A possible cause is by the reaction in the plating bath itself. In a hypophosphite-based bath, the hydrogen produced as a byproduct is in contact with the palladium allowing the formation of Pd-H. The removal of the sample from the hydrogen-rich environment of the plating bath causes phase transformation and film shrinkage (Cheng and Yeung, 2001). The autocatalytic reaction in the plating bath is given by the following equation.

$$Pd(NH_3)_4^{2+} + 2H_2PO_4^{2-} + 2H_2O^- \rightarrow Pd^0 + 4NH_3 + 2HPO_3^{2-} + 4H^+ + H_2 \quad (51)$$
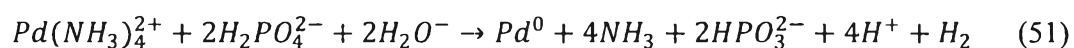
      The EDX analysis of the deposits indicated a high concentration of the palladium on the surface (95% wt), with a slight amount of phosphorus, which originated from the hypophosphite. Cheng et al. (2001) suggested the deposition of phosphorous along with palladium can result in the formation of Pd-

P alloys. The equation below demonstrates the proposed reaction of phosphorus formation.

$$PO_2^- + 3H^- + 2H_2O \rightarrow P + 4OH^- + 1.5H_2 \tag{52}$$
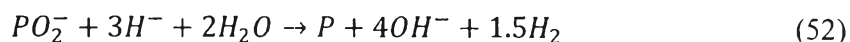
The average palladium particle size was found to be 500 nm in diameter. The FESEM image with higher resolution, 15000X magnifications, reveals the palladium particles in Figure 4.12.

The formation of an identical palladium layer for each experiment is a difficult task, mostly because the layer must be free of pores, cracks and well adhered to the steel surface.

### 4.1.4.2 Palladium Coated on a carbon steel tube

The surface of a plated carbon steel tube was examined under a scanning electron microscope (SEM). The tube was exposed to the atmosphere at high temperature during experiments performed before surface examination. Two sections were cut, one from the middle and one from the end for surface characterization purpose. Micrographs of the coating are shown in Figure 4.13 and Figure 4.14. The palladium deposit was partially coated on the surface. The palladium particles have largely filled the surface defects on the substrate revealed in Figure 4.15. The palladium deposit appears to consist of two regions: a nodule palladium particle in the surface defects and an uncoated area. An energy-dispersive X-ray (EDX) analysis of the deposit area indicated nearly pure of palladium, with a slight amount of phosphorus, which originated from the Hypophosphite. EDX analysis revealed that the uncoated region had formed an oxide layer, presumably a result of exposure to the atmosphere during the experiment.
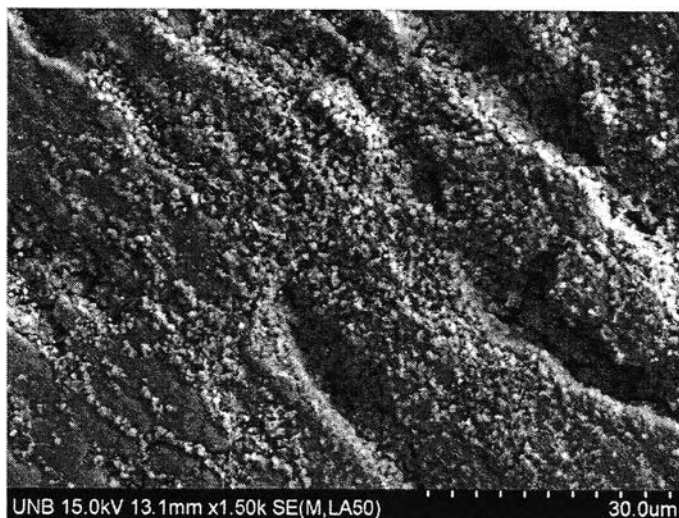
Figure 4.13 FESEM micrograph of an electroless plated carbon steel sample (1500X Magnification).
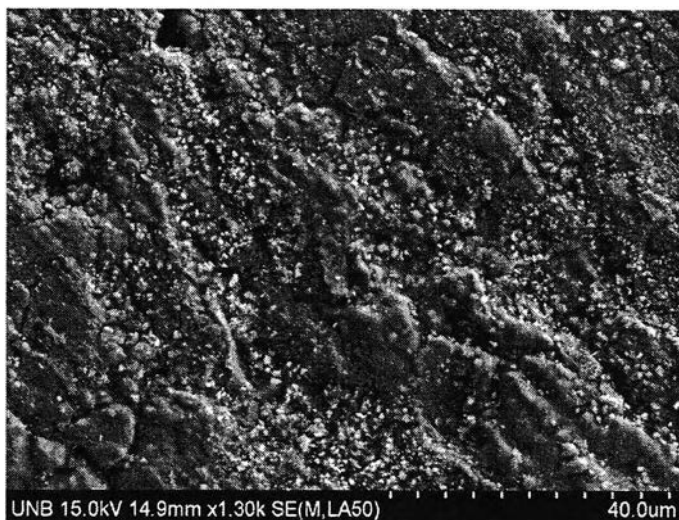
Figure 4.14 FESEM micrograph of an electroless plated carbon steel sample (1300X Magnification).
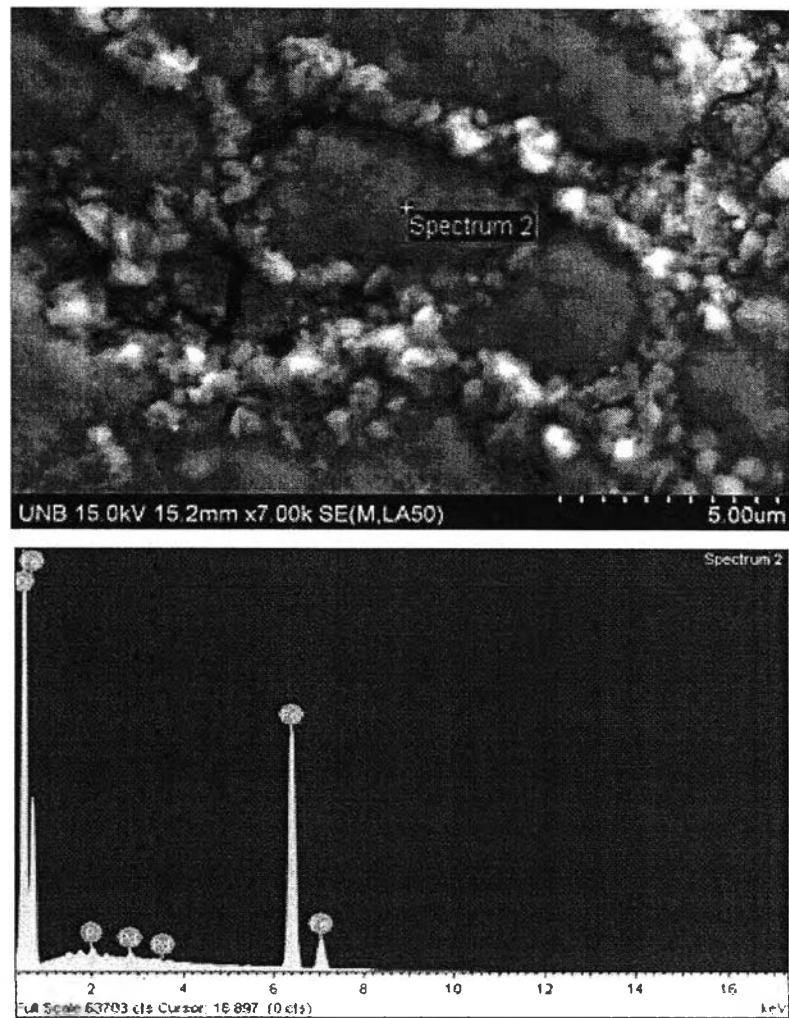
Figure 4.15 FESEM micrograph of an electroless plated carbon steel sample (7000X Magnification) with EDX result showing the presence of oxide scale.

The previous electroless plating on a carbon steel coupon (section 4.1.2.1) was well adhered and uniform. In case of the carbon steel tube, the solution and the plating conditions were similar to the small coupon. The palladium deposit on the plated tube was uneven compared to the plated coupon. It was probably caused by the distribution of palladium particles in the plating solution. Since the solution was not well mixed, the palladium film showed poor distribution of palladium particles on the carbon steel tube surface.

4.2 Hydrogen Permeation through Hastelloy

### 4.2.1 Minimum Temperature Limit

Test for the minimum temperature of hydrogen diffusion through Hastelloy were conducted at various temperatures. Hydrogen was injected into the system 864.74 kPa at ambient temperature. The testing apparatus was heated to the desired temperature. The first test was conducted at 200°C. This temperature gave no measurable diffusion rate through the steel. The test temperature was increased by 50°C increments. Therefore, the next test temperature was 250°C. At this temperature the hydrogen partial pressure in the sealed tube decreased at the rate of 6.51 kPa/hr. Therefore, the MTL is between $200 \leq T \leq 250$°C.

4.2.2 Hydrogen Diffusion through passive oxide layer

The outside surface of Hastelloy tube was as received. Before the permeation test begin, the inside surface of the tubular specimen was exposed to hydrogen purging to remove the oxide layer in order to eliminate the effect of an internal oxide layer. The purging step was conducted by passing 7.7 ml/min of hydrogen gas through the tube for 5 days at the temperature of 325°C. The oxide layer on the outside was allowed to form during the five days of heating.

Hydrogen was injected into the tube at the initial pressure of 818 kPa at room temperature. The tube was left for leak check for two days before the experiment begin. After no leak was found, the tube was heated to the desired temperature and kept at constant temperature throughout the test.

Tests were carried out at two temperatures, 250°C and 335°C. The decrease in hydrogen pressure with time for 250 and 335°C with an oxide layer on the outside is present in Figure 4.16. The permeation rate of hydrogen through Hastelloy varied with temperature. The decrease of hydrogen partial pressure at 250°C was lower than the decrease for the higher temperature as 335°C.
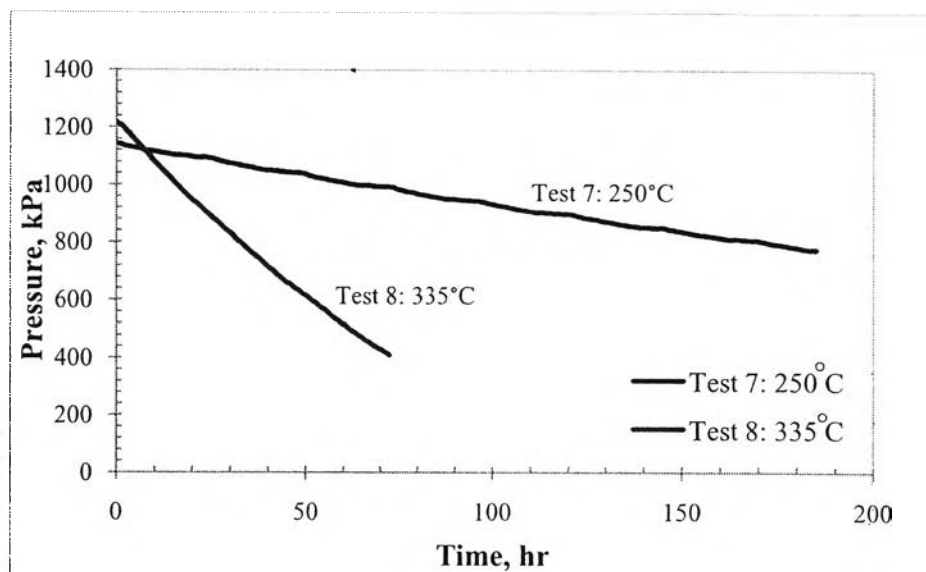
Figure 4.16 The change in hydrogen pressure inside the tube with time at the temperatures of 250°C and 335°C with the oxide layer on the outside and oxide layer removed from the inside.

Table 4.5 Summary of experimental data and constant value calculation

Test no.	Temp. (°C)	Initaial P (kPa)	Final P (kPa)	D_{app} Based on Fick's law $(m^2 s^{-1})$	D_{app} Based on Sievert's law $(m^2 s^{-1})$	Resistance $(s\,m^{-1})$
7	250	142.54	772.13	5.05×10^{-13}	3.10×10^{-7}	1.49×10^{9}
8	335	216.15	408.74	3.49×10^{-12}	8.70×10^{-7}	2.15×10^{8}

The apparent diffusivity and the resistance are presented in Table 4.5. The diffusivity and resistance are a function of temperature i.e., for 250°C the diffusivity reached is 5.05×10^{-13} m² s⁻¹, while for 335 °C the diffusivity is 3.49×10^{-12} m² s⁻¹. Conversely, the resistance decreased with an increase in temperature indicating hydrogen transport through Hastelloy increases with an increase in temperature.

4.2.3 Hydrogen Diffusion through Palladium coated Hastelloy

Tests were performed to determine the effect of coating Hastelloy on hydrogen transport through the metal.
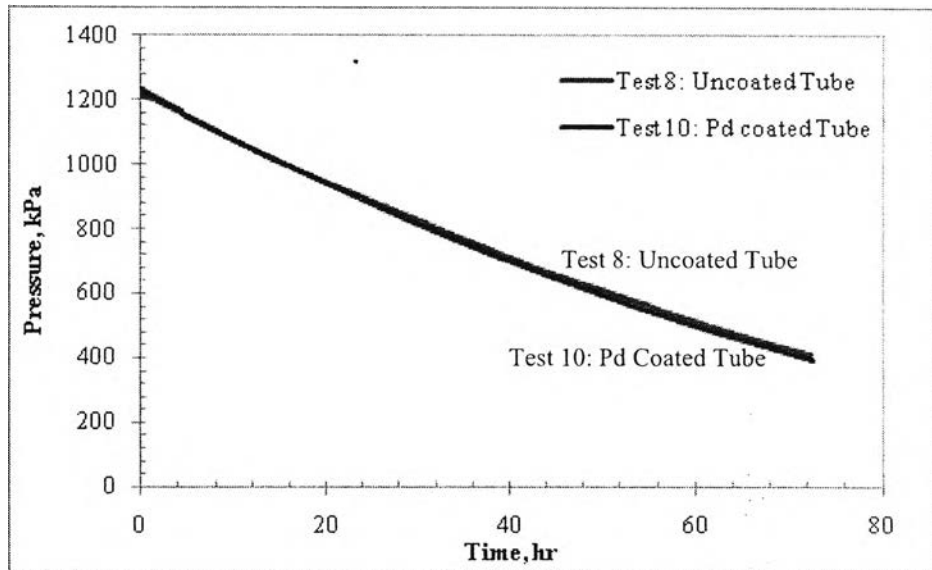
Figure 4.17 The comparison of hydrogen pressure with time at a temperature of 335°C with and without palladium coated on the outside surface.

Figure 4.17 demonstrates the result for a temperature of 335°C. The hydrogen partial pressure in the presence of palladium tube decreased from 1234.18 kPa to 394.63 kPa after 72 hours compared to the absence of palladium on the tube which decreased from 1216.15 kPa to 411.23 kPa after 72 hours. The change in pressure for the coated tube and uncoated tube was essentially the same. Thus, the presence of palladium on the external surface does not have an effect on the hydrogen transport through hastelloy at this temperature.

Table 4.6 Summary of experimental data for Hastelloy

| Test no.	Temp. (°C)	Initaial P (kPa)	Final P (kPa)	D_{app} Based on Fick's law ($m^2 s^{-1}$)	D_{app} Based on Sievert's law ($m^2 s^{-1}$)	Resistance (s m^{-1})
9	250	1148.71	678.14	5.35×10^{-13}	3.19×10^{-7}	1.40×10^{9}
10	335	1234.18	394.63	3.87×10^{-12}	9.48×10^{-7}	1.94×10^{8}

4.2.4   Surface Characterizations of Palladium on the Hastelloy tube

Bare hastelloy and a palladium film deposited on the hastelloy steel tube surface were evaluated by surface characterization techniques using a Field Emission Scanning Electron Microscopy (FESEM) investigation. Figure 4.18 demonstrates the morphology of the as received specimen. Energy Dispersive X-ray analysis (EDX) indicated the element composition of the alloy presented in Appendix A. As received tube surface was smooth and shiny. The parallel traces are present due to mechanically cleaning in order to facilitate the adherence of the deposit.

UNB 15.0kV 14.9mm x300 SE(M.LA50)   100um
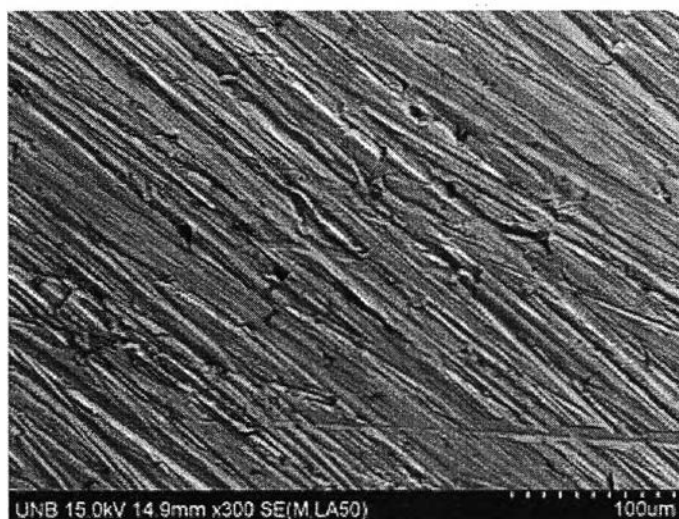
Figure 4.18 FESEM pictures of an unplated hastelloy C276 (300X Magnification).
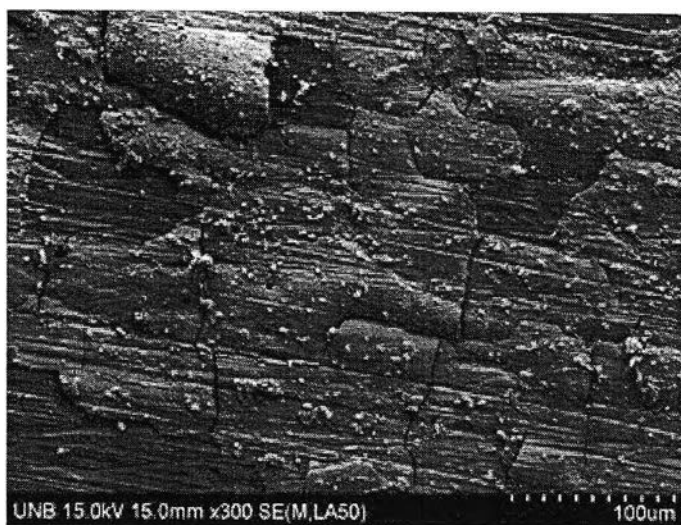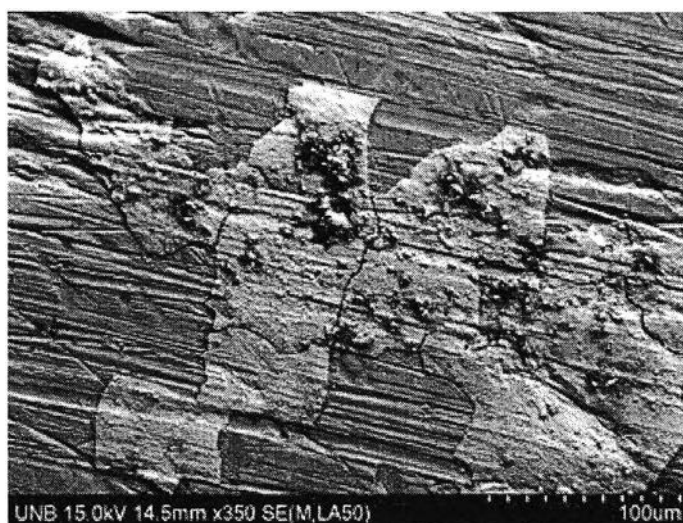
Figure 4.19 FESEM micrograph of electroless plated hastelloy sample (300X Magnification).
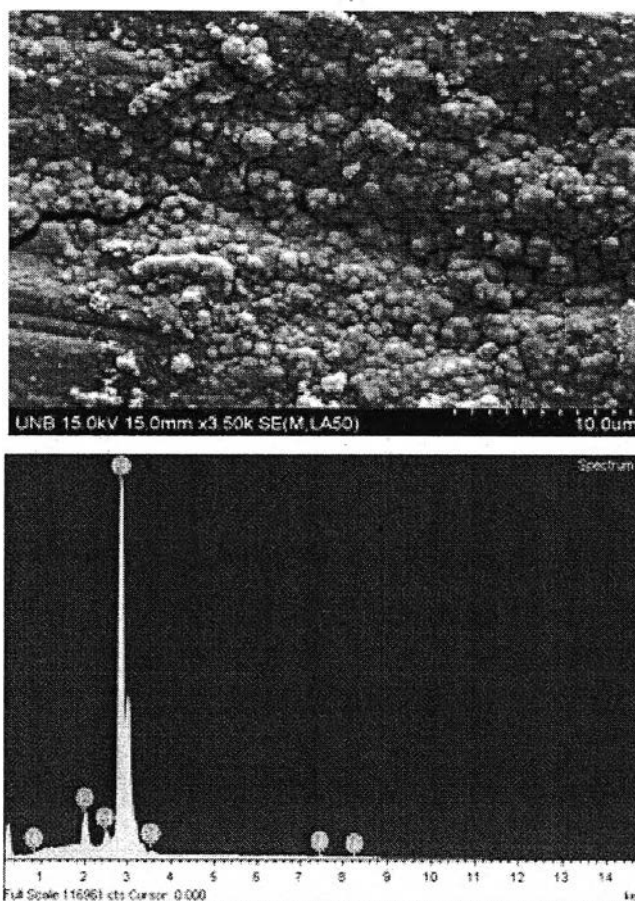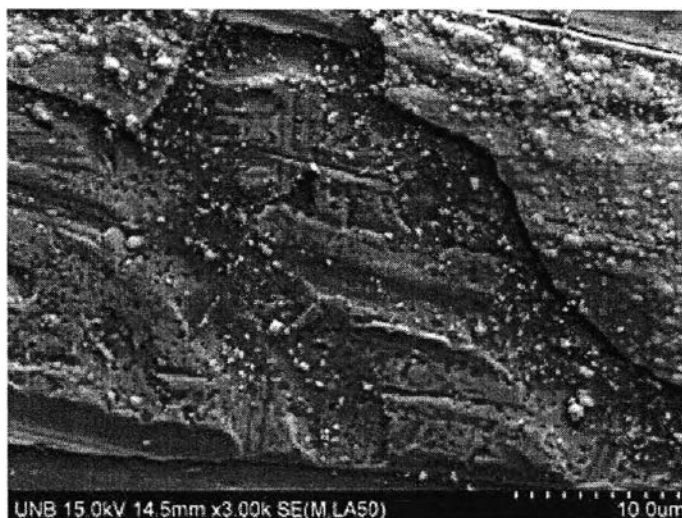

Figure 4.20 FESEM micrograph of electroless plated hastelloy sample (3500X Magnification) with EDX result showing the presence of oxide scale.

Figure 4.19 displays the palladium coating obtained by electroless deposition. A thin film was formed of palladium on hastelloy. It appears that the film was not well adhered to the tube surface. It displays a film with flakes. The deposit exhibited a crack pattern and isolated films from the substrate. Figure 4.20 demonstrates a higher magnified image of the film. An EDX analysis of the deposit indicated almost exclusively palladium with small amounts of phosphorus, which originated from the plating solution. The analysis also indicated the presence of nickel, which came from the steel matrix.

UNB 15.0kV 14.5mm x350 SE(M,LA50)   100um

Figure 4.21 FESEM micrograph of electroless plated hastelloy sample after scratching (350X Magnification).

The layer of palladium deposit was scratched in order to take off the non-adhered film. Figure 4.22 reveals the surface after scratching. Although some part of the film was removed, there is a continuous film of palladium which has good adhesion on the tube surface. The high magnification image in Figure 4.22 displays small palladium particle.

Figure 4.22 FESEM micrograph of electroless plated hastelloy sample after scratching (3000X Magnification).

It can be observed that the morphology of the film is highly dependent on the nature of the original surface of the substrate. The electroless plating technique performs well on a carbon steel substrate. However, the electroless plating technique may not be a suitable coating technique for hastelloy.

DISCUSSION

Gaseous permeation techniques rely on the dissociative chemisorptions on the surface, dissolution of atomic hydrogen on the surface into the bulk and diffusion of atomic hydrogen in the membrane (Barrer, 1951) and the reactions which occur conversely on the exit side of the tube. Diffusion of hydrogen through the metal also depends on the temperature since the transport of hydrogen in a metal lattice can be viewed as a thermally activated hopping process (Buckley, 2001). All activation energies for the steps involving hydrogen transport are significantly dependent on temperature.

The test materials were carbon steel A179 and hastelloy C276. Their elemental compositions are presented in Appendix A. Carbon steel is an iron based alloy whereas hastelloy is the nickel based alloy. Hydrogen permeation through carbon steel was found more rapid than hastelloy. Several studies have shown the crystal

structure of nickel, which is in Face-centered cubic (FCC), have lower hydrogen diffusivity and permeability than the structure of iron, which is body-centered cubic structure (BCC). Figure 4.23 displays the permeability constants for hydrogen in various metals as a function of temperature. It is apparent from the figure that iron, which is the main component in carbon steel, exhibits higher hydrogen permeability than nickel, which is the major component in hastelloy. SEM Image of grain size of an as received carbon steel and hastelloy were presented in Appendix H. The hastelloy seems to be more compact. It may affect the hydrogen penetration through the alloy.
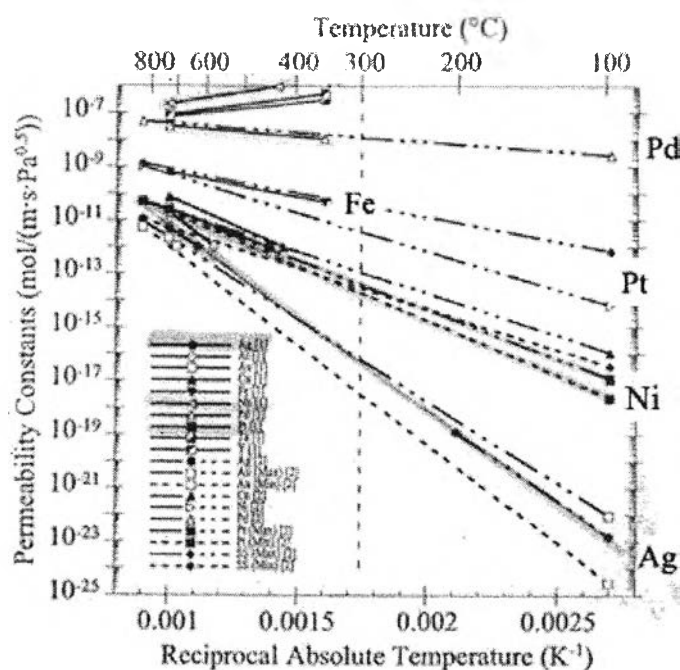
Figure 4.23 Permeability constants for hydrogen in various metals as a function of temperature (Gunter W.D., 1987).

In the case of carbon steel, our finding was the lowest temperature that gaseous hydrogen can diffuse through the carbon steel was $90 \leq T \leq 150°C$. The minimum temperature for Hastelloy was found to be $200 \leq T \leq 250°C$. Above these temperatures the molecular hydrogen has adequate energy to dissociative adsorb on the surface, dissociate and penetrate through the metal. Below this temperature, hydrogen diffusion was not detectable within two days.

To further investigate the role of oxide films on the outside surface of the steel, the outside passive oxide film was allowed to form spontaneously. Carbon steel at 150 and 250°C gave different values of diffusivity and resistance. At 250°C the diffusivity was an order of magnitude higher than at 150°C. In the case of hastelloy, the diffusivity at 250°C was one order of magnitude lower than at 335°C. As observed, the increase in temperature within the range of 85 to 100°C resulted in a significant increase in transport.

The oxide films, which occur spontaneously by air exposure, act as a significant barrier to hydrogen permeation. Although the diffusivity of hydrogen through the oxide film was small, the oxide film present on the carbon steel has a porous surface and crack like pattern as shown in Figure 4.4. The cracks may be a significant diffusion path for hydrogen from the metal. However, the presence of the oxide film on hastelloy was found to be more uniform. This type of film would not allow hydrogen to pass through cracks as were found on the carbon steel.

Swansiger et al. proposed the parallel processes of hydrogen diffusion through the oxides; (1) rate-limiting permeation through the thin oxide film, (2) transport through cracks or defects in the film followed by rate-limiting permeation through the substrate. The oxide acts as a significant barrier. Bruzzoni et al. (2000) mentioned that although the oxide at the exit surface had less impeding effect than on the entry surface, it can significantly reduce the permeation rate because the oxide causes resistance to the recombination reaction at the exit surface.

To promote the rapid permeation of hydrogen through the metal, a palladium coating was applied to the outside surface of the tube specimen. The following reactions are expected to be more rapid resulting with the palladium catalyst;

$$2H_{abs} \quad \rightarrow \quad H_{2\,surface} \quad\quad\quad (53)$$

$$H_{2\,surface} \quad \rightarrow \quad H_{2\,des} \quad\quad\quad (54)$$
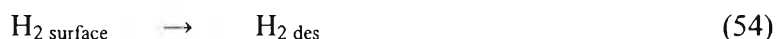
The plot of hydrogen partial pressure with time obtained for the palladium coated tube is compared to the uncoated tube. In case of carbon steel, the palladium coated on the external surface of tubes revealed a higher rate of hydrogen permeation compared to the uncoated tube. At 250°C the coated tube increased the permeation

rate by a factor of two compared to the uncoated tube. At 150°C the palladium coated tube increased the permeation rate by the factor of three. The permeation data for both cases demonstrate an increase in the diffusivity and a lower resistance. This is in good agreement with other works that suggested the palladium coated layer reduces the activation energy.

Shu et al. (1993) reported the activation energy of hydrogen diffusion through palladium electroless plated layer is much less than the bulk diffusion in homogeneous alloys. Moreover, covering the bare metal surface with a thin film of palladium can avoid the formation of a passive oxide film. For Hastelloy, the palladium coated surface showed a negligible increase in the rate of hydrogen permeation for both test temperatures. The pressure and time curve for the uncoated and coated tube gives very similar results. The diffusivity values of hastelloy were not affected by changed surface conditions. It was hypothesized that hastelloy forms a very thin oxide layer when exposed to the atmosphere which gives a specific resistance. Surface quality of the palladium coated film can also affect the rate of permeation. The palladium deposit on hastelloy revealed a film with flakes. Some part of the film was isolated from the substrate. The uneven surface may reduce the effect of palladium on hydrogen permeation. However, the hastelloy with different surface condition display no differences in permeation behavior. The rate controlling step for permeation through hastelloy seemed to be governed by bulk metal diffusion.

Our permeation results are compared with the results from previous studies shown in Table 4.7. Kongvarhodom et al. (2009) proposed the relationship of diffusivity as a function of temperature and gave the value of hydrogen diffusivity through carbon steel. The reported diffusivity varies over several orders of magnitude. This variation is possibly due to differences in the steel surface or steel preparation conditions. In deriving the equation used in the calculation of the diffusivity, it was assumed that a pseudo steady state exists. For the carbon steel values of the solubility of hydrogen in carbon steel justify this assumption but apparently not for hastelloy. The surface processes of hydrogen adsorption and desorption provide a significant resistance compared to the diffusion of hydrogen in the metal

Table 4.7 Comparison of permeation performance reported in literature

Metal Samples	Initial P (kPa)	T (K)	D_{app} (m/s)	Method	Ref.
Pt/carbon steel	950	580	8.1×10^{-10}	Gas phase permeation	(Kongvarhodom, 2009)
Pd/23%Ag	2000	580	1.2×10^{-7}	Gas phase permeation	(Meunier et al., 1981)
Monel	2000	580	3.7×10^{-11}	Gas phase permeation	(Meunier et al., 1981)
Annealed ultralow carbon steel	100	298	9.6×10^{-11}	Electro chemical permeation	(Yuan,2007)
Alpha iron/Pd	-	298	5.1×10^{-9}	Electro chemical permetaion	(Bruzzoni and Carranza, 2000)
Alpha iron	10-3000	573	5.7×10^{-8}	Gas phase permeation	(Nelson, 1973)
Low carbon steel	-	298	3.8×10^{-12}	Two-cell permeation technique	(M.J. Robinson, 2006)
316 Stainless steel	-	304	1.8×10^{-13}	Electro chemical permeation	(Kumar and Balasubramaniam, 1997)
Oxide film/carbon steel	1017	423	6.0×10^{-13}	Gas phase permeation	This study
Oxide film/carbon steel	1087	523	7.5×10^{-12}	Gas phase permeation	This study
Pd/ carbon steel	1016	423	2.5×10^{-12}	Gas phase permeation	This study
Pd/ carbon steel	1121	523	1.7×10^{-11}	Gas phase permeation	This study
Oxide film/Hastelloy	1142	523	5.0×10^{-13}	Gas phase permeation	This study
Oxide film/Hastelloy	1216	608	3.5×10^{-12}	Gas phase permeation	This study
Pd/ Hastelloy	1148	678	5.3×10^{-13}	Gas phase permeation	This study
Pd/ Hastelloy	1234	608	3.9×10^{-12}	Gas phase permeation	This study

4.3 Oxide Removal by Hydrogen Purging Method

There is an oxide film formed on the surface of both sides of tube. The films affect the hydrogen permeation as mentioned in section 2.5. During the experiment performed, 2.5% O_2 was in the test section and therefore forming an oxide film inside the tube, which is a barrier for hydrogen diffusion. The focus of this research is to evaluate the effect of the outside surface on hydrogen transport. The inner oxide film should therefore be eliminated to give consistent results.

Cheng et al. (2001) mentioned that iron oxide can be removed by hydrogen gas. Both reported an increase of oxide removal with an increase in hydrogen partial pressure. To test this hypothesis, an additional experiment was carried out. The hydrogen gas was purged through the tube with the flow rate of 7.7 ml/min (10 psig at the regulator scale). The purging duration was 5 days at the temperature of 325°C.
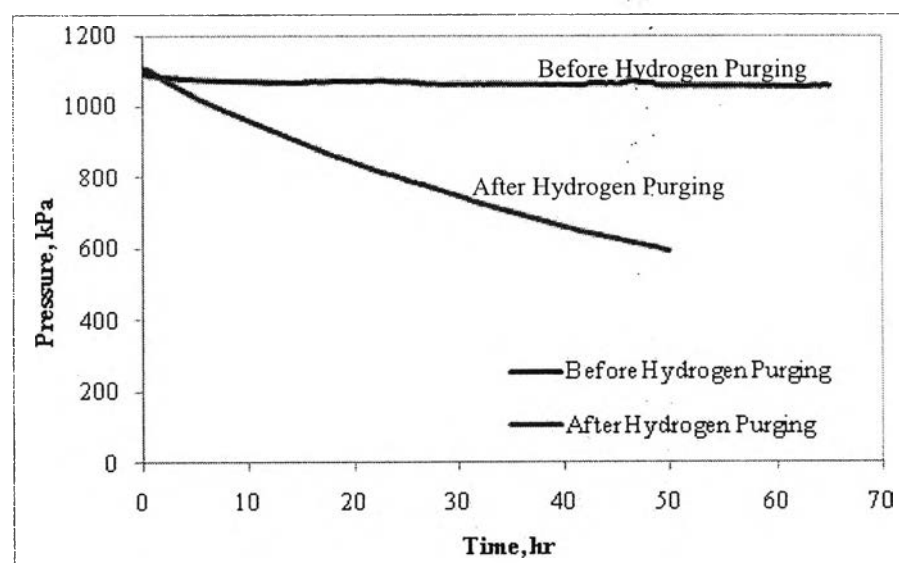
Figure 4.24 The hydrogen permeation rate with time at 250°C with two surface conditions; a mature oxide inside and a minimum oxide inside.

Figure 4.24 displays the comparison of hydrogen pressure reduction with time of the tube before and after purging with hydrogen. Referring to the before hydrogen purging curve, the pressure remains unchanged. It was identified that hydrogen cannot penetrate into the metal because the inner oxide layer blocked hydrogen passage. The

surface reaction $H_{2\,(g)} \rightarrow 2H_{ads\,(g)}$ was strongly retarded so hydrogen uptake would not be possible.

Table 4.8 Summary of experimental data and constant value calculation

	Temp. (°C)	Initaial P (kPa)	Final P (kPa)	D_{app} Based on Fick's law ($m^2 s^{-1}$)	D_{app} Based on Sievert's law ($m^2 s^{-1}$)	Resistance (s m^{-1})
Before Purging	250	1092.13	1045.42	6.39×10^{-14}	7.78×10^{-8}	1.18×10^{10}
After Purging	250	1111.32	557.52	2.47×10^{-12}	1.71×10^{-6}	3.04×10^{8}

After hydrogen purging for 5 days, the hydrogen pressure curve shown in Figure 4.24 shows a more rapid decrease. It was determined that hydrogen purging at the temperature of 325°C removed the oxide film which covered the inner surface. Bruzzoni et al. (2000) mentioned that hydrogen acts to reduce the oxide film. It can increase the flexibility and the amorphous character of the oxide layer. The increase in hydrogen permeation rate was accompanied by the increase in amorphous character increase. It cannot be said the oxide layer was completely removed. However, the removal was adequate to allow hydrogen passage through the steel. The experimental results and coefficients are summarized in Table 4.8.